Using the MFS for the analysis of the sound absorption by a porous plate containing a periodic array of inclusions

E. Perrey-Debain[a] and B. Nennig[b]

[a]Laboratoire Roberval, Rue Personne de Roberval, BP 20529 F-60205 Compiègne Cedex
[b]Laboratoire d'Ingénierie des Systèmes Mécaniques et des MAtériaux, Supméca - 3, rue Fernand Hainaut - 93407 St Ouen Cedex
emmanuel.perrey-debain@utc.fr

The Method of Fundamental Solutions (MFS) is now a well-established technique that has proved to be reliable for a specific range of wave problems such as the scattering of acoustic and elastic waves by scatterers of regular shapes or by gratings. The aim of this work is to show that the technique can be used to model absorption problems whereby an incident acoustic wave impinges on a porous slab of finite thickness in which periodic inclusions are embedded. In the present work, the analysis is limited to the periodic array of rigid scatterers of various shape. The extension of the MFS to periodic problems is obtained by using appropriate periodic Greens functions for which highly convergent series exist. The influence of the inclusions is illustrated on various examples in order to enhance the absorption properties in the low frequency range or around specific frequency ranges.

1 Introduction

Porous materials are now widely used in different applications for passive noise reduction and control. The type of applications ranges from room acoustics predictions, sound proofing of aircrafts or cars' passenger compartments to muffler designs in HVAC systems. In many cases of practical interest, the acoustic treatment consists of thick layer of porous absorbing material backed by a rigid wall. Though efficient, these materials are known to exhibit poor acoustic performances at low frequencies. Because of these limitations, the use of multilayer materials have been investigated. An alternative solution is to embed periodic inclusions into the porous layer in order to provide additional energy scattering and dissipation mechanisms. Some measurements concerning these multi-scale materials have been carried out in the specific case of rigid inclusions [1] showing the interest for this concept. In practice, there is a need for efficient numerical tools or models in order to obtain an accurate prediction of the acoustic performances for such materials. When inclusions are of circular shapes, semi-analytical models are available [2]; a coupled mode formalism has also been presented in [1]. More generally, the Finite Element Method (FEM) remains the ultimate tool for such purpose as the method offers almost unlimited flexibility [3]. However, it can prove cumbersome and time-consuming both in terms of data preparation and computation especially when the frequency increases. This can have a negative impact when some efficient optimizations regarding, for instance, the geometry and position of the inclusions are needed. In a recent paper [4], the present authors investigated the use of the Method of Fundamental Solution (MFS) for solving single and multiple scattering problems involving obstacles filled with a poroelastic material. The method relies on placing an appropriate set of sources within and around the scatterer and calculate the amplitudes of these sources after applying the continuity equation on the scattering surface. Results showed the advantages offered by this method both in terms of data reduction and computational time for a wide range of obstacles with 'reasonable shapes'. In the present paper, the method is modified to take into account the effect of periodical array of rigid inclusions embedded in a porous slab of finite thickness installed on a rigid wall. The computational model is simplified by assuming that the material reacts like an equivalent fluid so only pressure waves are allowed to propagate in the material. For a brief nomenclature, we call ρ_p, k_p, the density and the wavenumber associated with the porous material. Similarly, ρ_0, k_0 refers to the air domain, in all cases we adopt the $\mathrm{e}^{-\mathrm{i}\omega t}$ convention.

2 Formulation

The geometry of the problem is depicted in Fig. 1. It consist of a two-dimensional porous slab Ω_p of thickness h with rigid backing (here at $x_2 = -h$, where $\mathbf{x} = x_1\mathbf{e}_1 + x_2\mathbf{e}_2$). The inclusion of boundary surface Γ_s is assumed perfectly rigid and the geometry is assumed d-periodic in the $\mathbf{e}_1$ direction. When the array is illuminated by a plane wave of angle of incidence θ^{inc}:

$$p_0^{\mathrm{inc}}(\mathbf{x}) = \frac{A^{\mathrm{inc}}}{\sqrt{d}}\mathrm{e}^{\mathrm{i}\alpha x_1}\mathrm{e}^{-\mathrm{i}\beta_0^0 x_2}, \tag{1}$$

then the solution of the scattering problem is pseudo-periodic, that is d-periodic with a phase shift, and the pressure must fulfill the condition

$$p(\mathbf{x} + md\,\mathbf{e}_1) = p(\mathbf{x})\mathrm{e}^{\mathrm{i}m\alpha d}. \tag{2}$$

Here m is a relative integer and

$$(\alpha, -\beta_0^0) = k_0(\sin\theta^{\mathrm{inc}}, -\cos\theta^{\mathrm{inc}})$$

is the incident wave-number vector. In the surrounding fluid domain Ω_0, the total pressure is split as $p_0 = p_0^{\mathrm{sc}} + p_0^{\mathrm{inc}}$ where the scattered field has the Floquet decomposition [5]:

$$p_0^{\mathrm{sc}}(\mathbf{x}) = \sum_{n\in\mathbb{Z}} \frac{A_n^0}{\sqrt{d}}\mathrm{e}^{\mathrm{i}\alpha_n x_1}\mathrm{e}^{\mathrm{i}\beta_n^0 x_2} \tag{3}$$

where $\alpha_n = \alpha + n\frac{2\pi}{d}$ and $\beta_n^0 = \sqrt{k_0^2 - (\alpha_n)^2}$ can be either real (i.e. a propagating wave) or imaginary (i.e. an evanescent wave). Similarly, the pressure field in the slab can be decomposed as $p_p = p_p^{\mathrm{r}} + p_p^{\mathrm{s}}$. The field p_p^{r} stands for the regular part:

$$p_p^{\mathrm{r}}(\mathbf{x}) = \sum_{n\in\mathbb{Z}} \frac{A_n^p}{\sqrt{d}}\mathrm{e}^{\mathrm{i}\alpha_n x_1}\left(\mathrm{e}^{\mathrm{i}\beta_n^p(x_2+2h)} + \mathrm{e}^{-\mathrm{i}\beta_n^p x_2}\right) \tag{4}$$

where $\beta_n^p = \sqrt{k_p^2 - \alpha_n^2}$. Note that the previous expansion takes into account the presence of the hard wall as $\partial_{x_2} p_p^{\mathrm{r}} = 0$ at $x_2 = -h$.The singular part p_p^{s} can be interpreted as the field scattered by the rigid inclusions. The main idea of the MFS is to seek the scattered field in the form of a distribution of Q monopoles:

$$p_p^{\mathrm{s}}(\mathbf{x}) = \sum_{q=1}^{Q} B_q G_{\alpha,w}^d(\mathbf{x}, \mathbf{y}_q). \tag{5}$$

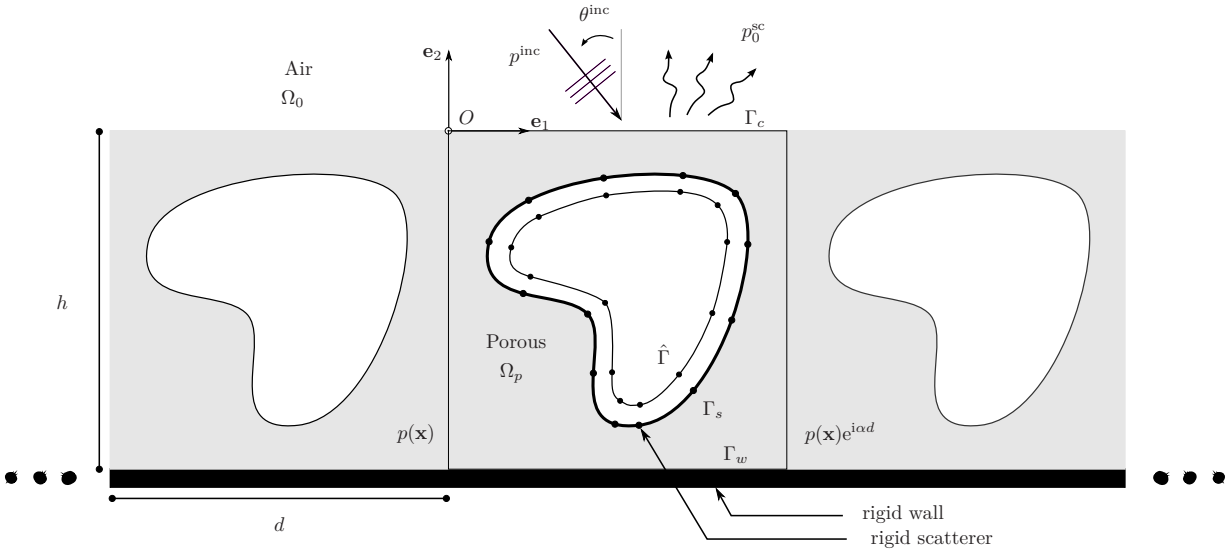

Figure 1: Geometry of the periodic cell.

Here the source points $\mathbf{y}_q$ are chosen to be located on a fictitious curve $\hat{\Gamma}$ within the inclusion and B_q are unknown coefficients. Function $G^d_{\alpha,w}(\mathbf{x},\mathbf{y})$ stands for the hard-wall periodic Green's function

$$G^d_{\alpha,w}(\mathbf{x},\mathbf{y}) = G^d_\alpha(\mathbf{x},\mathbf{y}) + G^d_\alpha(\mathbf{x},\mathbf{y}'), \tag{6}$$

where $\mathbf{y}'$ is the image source $\mathbf{y}' = (y_1, -y_2 - 2h)$ and $G^d_\alpha(\mathbf{x},\mathbf{y})$ is the classical Green's function in periodic domains [5]

$$G^d_\alpha(\mathbf{x},\mathbf{y}) = -\frac{\mathrm{i}}{4}\sum_{m\in\mathbb{Z}} H^1_0(k_p r_m)\mathrm{e}^{\mathrm{i}m\alpha d}. \tag{7}$$

Here, H^1_0 is the Hankel function of the first kind, $r_m = (\delta_2^2 + (\delta_1 - md)^2)^{1/2}$ is the distance between the field point and the source point of the m^{th} scatterer and $(\delta_1, \delta_2) = \mathbf{x} - \mathbf{y}$ corresponds to the distance on the generic cell $m = 0$. The series (7) is unfortunately very slowly convergent and is therefore not appropriate for numerical computations. In [5], the author has compared several methods to efficiently compute the periodic Green's function (7). Through extensive numerical tests it was shown that the Ewald method probably offers the best trade-off between computational time and robustness. This is based on the alternative form for Green's function [5]:

$$\begin{aligned} G^d_\alpha(\mathbf{x},\mathbf{y}) = \frac{1}{4d}\sum_{n\in\mathbb{Z}} \frac{\mathrm{e}^{\mathrm{i}\alpha_n\delta_1}}{\mathrm{i}\beta^p_n}\Bigg[&\mathrm{e}^{-\mathrm{i}\beta^p_n\delta_2}\mathrm{erfc}\left(-\frac{\mathrm{i}\beta^p_n d}{2e} + \frac{e\delta_2}{d}\right) \\ &+ \mathrm{e}^{\mathrm{i}\beta^p_n\delta_2}\mathrm{erfc}\left(-\frac{\mathrm{i}\beta^p_n d}{2e} - \frac{e\delta_2}{d}\right)\Bigg] \\ &+ \sum_{m\in\mathbb{Z}}\sum_{n=0}^{\infty}\frac{\mathrm{e}^{\mathrm{i}m\alpha d}}{4\pi n!}\left(\frac{k_0 d}{2e}\right)^{2n} E_{n+1}\left(\frac{e^2 r_m^2}{d^2}\right). \end{aligned} \tag{8}$$

The advantage of such a representation is that the series is quickly convergent and only a small number of terms is needed to achieve extremely accurate results (to double standard precision if necessary). Furthermore, the complementary Error function erfc and the exponential integral E_n can be computed quickly [6]. In (8), the positive constant e is arbitrary though its value will affect the convergence of the two summations, this is discussed in [5] and references therein. As shown in Table 3 in [5], $e = 4$ seems to be a good choice allowing fast convergence and it was observed that less than twenty terms are required in the two summations over m and around ten in the summation over n to nearly achieve machine precision.

The first set of equations is obtained after applying the classical continuity conditions at the air-porous interface Γ_c, that is $p_0 = p_p$ and $\rho_0^{-1}\partial_{x_2} p_0 = \rho_p^{-1}\partial_{x_2} p_p$ with $x_2 = 0$. At the interface, it is more advantageous to use the the Floquet mode representation for the Green's function representation [5]

$$G^d_\alpha(\mathbf{x},\mathbf{y}) = \frac{1}{2d}\sum_{n\in\mathbb{Z}} \frac{\mathrm{e}^{\mathrm{i}\beta^p_n|\delta_2|}\mathrm{e}^{\mathrm{i}\alpha_n\delta_1}}{\mathrm{i}\beta^p_n}, \tag{9}$$

so that we can invoke the orthogonality of the Floquet modes to give

$$A^0_n + \delta_{0n}A^{\text{inc}} = A^p_n\left(\mathrm{e}^{\mathrm{i}\beta^p_n 2h} + 1\right) + \sum_{q=0}^{Q} C_{nq}\, B_q \tag{10}$$

and

$$R_n\left(A^0_n - \delta_{0n}A^{\text{inc}}\right) = A^p_n\left(\mathrm{e}^{\mathrm{i}\beta^p_n 2h} - 1\right) + \sum_{q=0}^{Q} C_{nq}\, B_q \tag{11}$$

with $R_n = (\rho_p\beta^0_n)/(\rho_0\beta^p_n)$ and

$$C_{nq} = \cos\left[\beta^p_n\left(y_{q_2} + h\right)\right]\frac{\mathrm{e}^{-\mathrm{i}\alpha_n y_{q_1} + \mathrm{i}\beta^p_n h}}{\mathrm{i}\beta^p_n\sqrt{d}} \tag{12}$$

In these equations, n ranges from $-N$ to N so the number of Floquet modes is $2N + 1$. The second set of equations is obtained by applying the rigid boundary conditions at some collocation points $\mathbf{x}_j$, $j = 1, \ldots J$ located on the surface of the inclusion Γ_s:

$$\partial_n p_p(\mathbf{x}_j) = \partial_n p^{\text{r}}_p(\mathbf{x}_j) + \partial_n p^{\text{s}}_p(\mathbf{x}_j) = 0 \tag{13}$$

where n is the normal unit vector.

Once the wave amplitudes have been evaluated, the integration of the acoustic intensity over the unit cell

using the orthogonality relation of the Floquet modes given in (3) leads to the energy balance:

$$\mathcal{A} + \mathcal{R} = 1, \tag{14}$$

where the energy reflection coefficient $\mathcal{R}$ is defined as the ratio of the scattered power in the x_2 direction

$$\mathcal{P}_r = \sum_{n\in\mathbb{Z}} \mathfrak{Re}\left\{\beta_n^0\right\} |A_n^0|^2/(\rho_0\omega), \tag{15}$$

to the incident power

$$\mathcal{P}_i = |A^{\text{inc}}|^2 k_0/(\rho_0\omega). \tag{16}$$

3 Results

In this section, numerical results of practical interest concerning rigid inclusions of circular and elliptical shape are presented. In particular, we shall focus on the evaluation of the absorption coefficient $\mathcal{A} = 1 - \mathcal{R}$ which is the quantity of interest. Numerical aspects of the method such as the convergence analysis and the conditioning of the algebraic system shall not be discussed here as this should be the subject for a separate paper. The configuration studied here is somewhat similar to the one from [2]. It consists of porous slab of thickness $h = 2$ cm made with Fireflex (Recticel, Belgium). For the sake of completeness, the material characteristics are reminded here: porosity $\phi = 0.95$, flow resistivity $\sigma = 8900$ Nm^{-4}s, viscous and thermal characteristic lengths $\Lambda = 180\mu$m and $\Lambda' = 360\mu$m and the tortuosity $\alpha_{\text{inf}} = 1.42$.

The first example concerns that of an incoming pressure wave of normal incidence ($\theta^{\text{inc}} = 0$). Four type of inclusions are considered: a circular one with radius 7.5 mms, and three elliptical inclusions with different inclinations as depicted in Fig. 2. The source points location for the expansion of the singular field in the porous slab is also shown. Black arrows represent the local unit normal vectors at collocation points. In all cases, the total number of degrees of freedom does'nt exceed 40, that is around 30 source points and 5 Floquet modes.

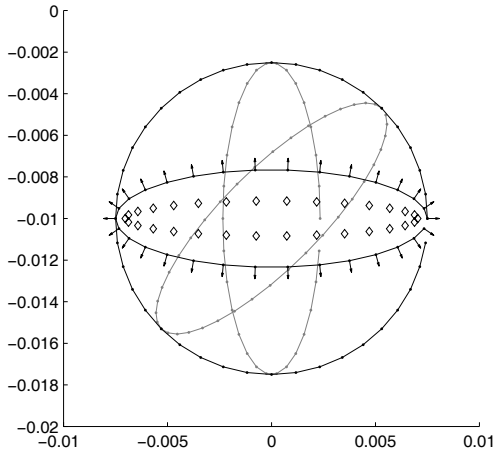

Figure 2: Circular and elliptical inclusions with different inclinations.

Fig. 3 shows the absorption coefficients for different type of inclusions. Because there is no exact solutions for these configurations, except maybe for the circular inclusion, the reference solutions are computed using a finite element model. The computations are carried out using Lagrange quadratic finite elements for the description of the acoustic pressure in both domains. For the radiation condition of the scattered field in the air domain, we choose to use the Dirichlet to Newman (DtN) map based on the Floquet decomposition Eq. (3). This approach was favored here as the use of the PML technique is not efficient for 'low-frequency' applications, i.e. when the wavelength is large compared to the size of the computational domain (the dimension of a unit cell is about $2-3$ cms). The number of finite elements used in order to capture the geometry of the inclusions is about 1000. The comparisons between the two methods are excellent and this makes the MFS a good candidate for solving this type of problems. The overall computational time (using the MFS) is about 0.1 s per frequency. On can identify the appearance of the second Floquet mode ($|n| = 1$) around $f = c_0/d \approx 17000$ Hz (here $d = 2$ cm). These early results suggest that the horizon-

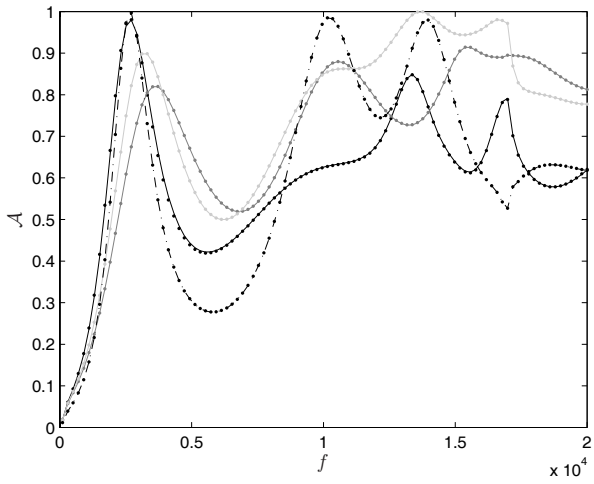

Figure 3: Absorption coefficients for different type of inclusions when the porous slab is excited at normal incidence. Results are computed with the MFS (lines) and with the FEM (dots). The type of inclusion is identified by the color: horizontal ellipse (black), vertical ellipse (dark grey), oblique (light grey), circle (dash-dot).

tal elliptical inclusion shows quite good performance in the low frequency range. It is interesting to see how this is modified when the slab is illuminated under oblique incidence. In this regard, Fig. 4 shows the absorption coefficient in function of the frequency and the angle of incidence. This shows good performance in the interval $f \in$ [2000 Hz, 4000 Hz] irrespective of the incident wave with a peak of absorption close to unity around 3000 Hz. For the sake of comparison, results concerning the homogeneous slab (no inclusion) are also shown in Fig. 5. We may notice a similar dip around 5000-6000 Hz when $\theta^{\text{inc}} \in [0, \pi/4]$. This drop in performance has been observed for various shapes.

The last numerical experiment concerns the scatter-

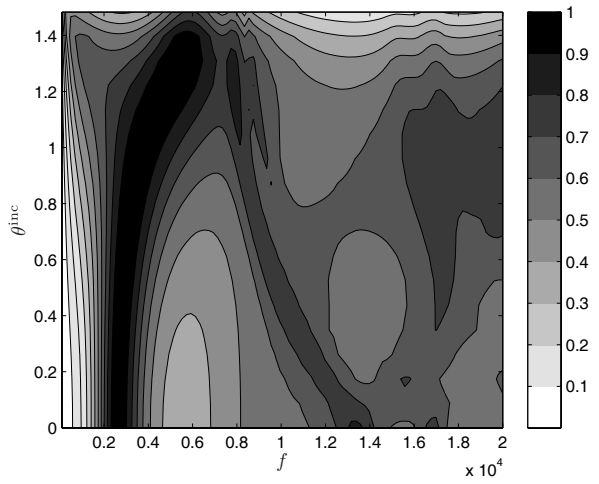

Figure 4: Plot of the absorption coefficient in function of the frequency and the angle of incidence (horizontal elliptical inclusion).

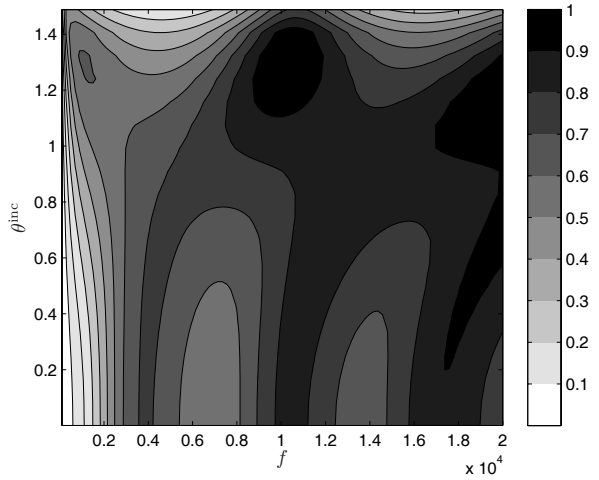

Figure 5: Plot of the absorption coefficient in function of the frequency and the angle of incidence (homogeneous slab).

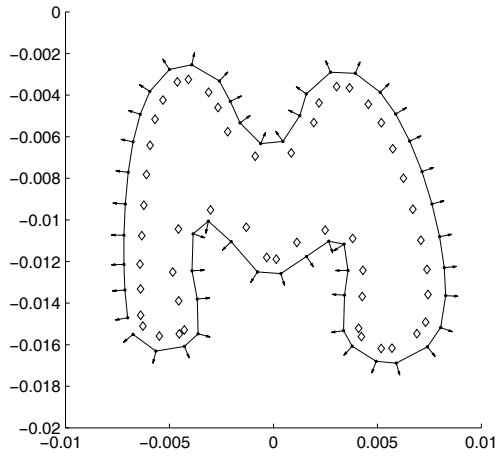

Figure 6: 'M'-shaped rigid inclusion.

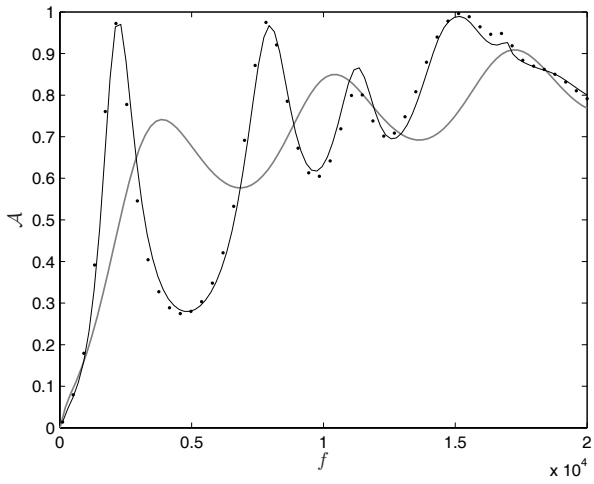

Figure 7: Absorption coefficients for the letter 'M' when the porous slab is excited at normal incidence. Results are computed with the MFS (lines) and with the FEM (dots). The grey line refers to the homogeneous slab.

ing by a non-convex rigid inclusion having the shape of letters 'M'. The boundary has been drawn using a graphical software and interpolated with Bezier curves. Fig. 6 shows the locations of the source points as well as the collocation points. Here again, the MFS resulting algebraic system is of very small size as the number of source points does not exceed 60.

Fig. 7 shows the absorption coefficients when the slab is illuminated by a normal incident plane wave. The comparison with the FEM results shows reasonably good agreement from an engineering point of view although small discrepancies are clearly visible. The reasons for this are not entirely clear yet as similar calculations (in a somewhat different context) presented in [4] did not show such differences.

4 Conclusion

The application of the MFS for the acoustic wave scattering by a porous slab of finite thickness in which periodic rigid inclusions are embedded has been presented. Through many illustrative examples of increasing difficulty, comparisons with results computed using a finite element formulation illustrate the advantages of the method both in terms of computational resources and mesh preparation. It is hoped that the benefit of the MFS should be even bigger when dealing with poroelastic materials and/or for 3D configurations.

References

[1] B. Nennig, Y. Renou, J.-P. Groby, Y. Aurégan, "A mode matching approach for modeling two dimensional porous grating with infinitely rigid or soft inclusions", *J. Acoust. Soc. Am.*, in press.

[2] J.-P. Groby, O. Dazel, A. Duclos, L. Boeckx, W. Lauriks, "Enhancing absorption coefficient of a backed rigid frame porous layer by embedding

circular periodic inclusions", *J. Acoust. Soc. Am.* **130**(6), 3771-3780 (2011)

[3] J.-F. Allard, N. Atalla, *Propagation of sound in porous media: modelling sound absorbing materials*, John Wiley & Sons, (2009).

[4] B. Nennig, E. Perrey-Debain, J.-D. Chazot, "The method of fundamental solutions for acoustic wave scattering by a single and a periodic array of poroelastic scatterers", *Engineering Analysis with Boundary Elements*, **35**(8), 1019-1028 (2011).

[5] C.M. Linton, "The Green's function for the two dimensional Helmholtz equation in periodic domains",*J. Enging. Math.* **33**, 377-402 (1998).

[6] S. Zhang, J. Jin, *Computation of special functions*, Wiley (1996).